Advanced Functional Materials

Formation of a Quasi-Free-Standing Single Layer of Graphene and Hexagonal Boron Nitride on Pt(111) by a Single Molecular Precursor

--Manuscript Draft--

Manuscript Number:	adfm.201503591R2
Full Title:	Formation of a Quasi-Free-Standing Single Layer of Graphene and Hexagonal Boron Nitride on Pt(111) by a Single Molecular Precursor
Article Type:	Full Paper
Section/Category:	
Keywords:	EELS; plasmons; intensity-voltage LEEM; hexagonal in-plane heterostructures
Corresponding Author:	Elena Magnano, Dr. IOM CNR, Laboratorio TASC Trieste, ITALY
Additional Information:	
Question	**Response**
Please submit a plain text version of your cover letter here. **If you are submitting a revision of your manuscript, please do not overwrite your original cover letter. There is an opportunity for you to provide your responses to the reviewers later; please do not add them here**.	Dear Editor, enclosed for your consideration is the manuscript entitled “Formation of a quasi-free-standing single layer of graphene and hexagonal boron nitride on Pt(111) by a single molecular precursor” by S. Nappini et al. Research in graphene (G)-based photonics and electronics is currently facing the challenge of adapting the electronic properties of this material to a wide range of applications. Here we report a novel bottom-up approach to obtain a continuous almost free-standing hexagonal single layer with perfectly merging G and hexagonal boron-nitride (h-BN) domains using only one molecular precursor. This straightforward growth method is easily adaptable to industrial processes aiming at engineering the band gap of G by merging in the same layer the isostructural h-BN characterized by very different carrier mobility due to its wide bandgap. Up to now, however, G-h-BN layers have been obtained only by complicated routes, starting from two or three precursors or growing h-BN on existing G patches and viceversa. We demonstrate that a simple thermal decomposition of dimethylamine borane is sufficient to obtain a G-h-BN layer on Pt(111). For these reasons, we are confident that our manuscript meets all the criteria for publication in Advanced Functional Materials Sincerely yours, Elena Magnano, Federica Bondino and coauthors
Corresponding Author Secondary Information:	
Corresponding Author's Institution:	IOM CNR, Laboratorio TASC
Corresponding Author's Secondary Institution:	
First Author:	Silvia Nappini
First Author Secondary Information:	
Order of Authors:	Silvia Nappini
	Igor Pis
	Onur Tevfik Mentes

	Alessandro Sala
	Mattia Cattelan
	Stefano Agnoli
	Federica Bondino
	Elena Magnano, Dr.
Order of Authors Secondary Information:	
Abstract:	We show that on Pt(111) it is possible to prepare hexagonal boron nitride (h-BN) and graphene (G) in-plane heterojunctions from a single molecular precursor, by thermal decomposition of dimethylamine borane (DMAB). Photoemission, near-edge x-ray absorption spectroscopy, low energy electron microscopy and temperature programmed desorption measurements indicate that the layer fully covers the Pt(111) surface. Evidence of in-plane layer continuity, and weak interaction with Pt substrate has been established. Our findings demonstrate that dehydrogenation and pyrolitic decomposition of DMAB is an efficient and easy method for obtaining a continuous almost freestanding layer mostly made of G, h-BN with only a low percentage (<3%) of impurities (B and N-doped G domains or C-doped h-BN or BNC at the boundaries) in the same two dimensional sheet on a metal substrate, such as Pt(111), paving the way for the advancement of next-generation G-like-based electronics and novel spintronic devices.

WILEY-VCH

DOI: 10.1002/ adfm.201503591

Full Paper

Formation of a Quasi-Free-Standing Single Layer of Graphene and Hexagonal Boron Nitride on Pt(111) by a Single Molecular Precursor

Silvia Nappini, Igor Píš, Tefvik Onur Menteş, Alessandro Sala, Mattia Cattelan, Stefano Agnoli, Federica Bondino, Elena Magnano**

Dr. S. Nappini
IOM CNR laboratorio TASC, Basovizza (TS), 34149, Italy
E-mail: nappini@iom.cnr.it
Dr. I. Píš
Elettra - Sincrotrone Trieste, S.C.p.A., Basovizza (TS), 34149, Italy
E-mail: igor.pis@elettra.eu
Dr. T. O. Menteş
Elettra - Sincrotrone Trieste, S.C.p.A., Basovizza (TS), 34149, Italy
E-mail: tevfik.mentes@elettra.eu
Dr. A. Sala
Elettra - Sincrotrone Trieste, S.C.p.A., Basovizza (TS), 34149, Italy
E-mail: alessandro.sala@elettra.eu
M. Cattelan
Department of Chemical Sciences, University of Padua, Padova, , 35131, Italy
E-mail: mattia.cattelan.1@studenti.unipd.it
Dr. S. Agnoli
Department of Chemical Sciences, University of Padua, Padova, , 35131, Italy
E-mail: stefano.agnoli@unipd.it
Dr. F. Bondino
IOM CNR laboratorio TASC, Basovizza (TS), 34149, Italy
E-mail: bondino@iom.cnr.it
Dr. E. Magnano
IOM CNR laboratorio TASC, Basovizza (TS), 34149, Italy
Department of Physics, University of Johannesburg, PO Box 524, Auckland Park 2006, South Africa
E-mail: magnano@iom.cnr.it

Keywords: EELS, plasmons, intensity-voltage LEEM, hexagonal in-plane heterostructures

We show that on Pt(111) it is possible to prepare hexagonal boron nitride (h-BN) and graphene (G) in-plane heterojunctions from a single molecular precursor, by thermal decomposition of dimethylamine borane (DMAB). Photoemission, near-edge x-ray absorption spectroscopy, low energy electron microscopy and temperature programmed desorption measurements indicate that the layer fully covers the Pt(111) surface. Evidence of in-plane layer continuity, and weak interaction with Pt substrate has been established. ~~The~~

~~experimental results show that G and h-BN domains in the hybrid layer, although similar to the pure G and pure h-BN on Pt(111), show additional spectroscopic features which are consistent with the presence of impurities (N, B and h-BN) inside the G domains.~~ Our findings demonstrate that dehydrogenation and pyrolitic decomposition of DMAB is an efficient and easy method for obtaining a continuous almost freestanding layer mostly made of G, h-BN with only a low percentage (<3%) of impurities (B and N-doped G domains or C-doped h-BN or BNC at the boundaries) in the same two dimensional sheet on a metal substrate, such as Pt(111), paving the way for the advancement of next-generation G-like-based electronics and novel spintronic devices.

1. Introduction

Hexagonal boron nitride (*h*-BN) and graphene (G) are honeycomb atomic monolayer materials with identical structure and very similar lattice parameters (less than 1.7% mismatch). G has gained a clear prominence among materials thanks to its superb carrier mobility, good transparency, excellent thermal conductivity, in-plane mechanical strength, and chemical inertness. *h*-BN shares several of these properties, but, at variance with G, is an insulator with a wide band gap. Owing to the same structure, but very different carrier mobility, the possibility to merge these two materials into vertically stacked layers or lateral in-plane hybrid heterostructures is raising a great deal of interest in the prospect, for example, of building 2D atomic-layer circuits[1] or magnetic nanostructures at the *h*-BN/G interface[2], tailoring the conducting properties of G and engineering the band gap[3–6]. Up to now, *h*-BN-G in-plane hybrid structures have been obtained by using chemical vapor deposition (CVD) starting from two or three precursors[3–5], plasma-assisted deposition, mechanical transfer or a two step process consisting in the growth of *h*-BN on existing G patches[7–10] or the growth of *G* on *h*-BN patches created by etching reaction[11]. The atomic continuity of the *h*-BN and G

domains has been recently investigated on a local basis by scanning tunneling microscopy[7,9,12].

Here we report a novel approach to obtain continuous hybrid hexagonal heterostructures combining *h*-BN and G within the same two dimensional (2D) sheet (*h*-BNG layer) on single crystals in ultra-high-vacuum (UHV) environment by using only one molecular precursor, dimethylamine borane (DMAB). This growth route allows an easy and controlled preparation of a continuous almost freestanding layer mostly composed by G and *h*-BN with a very limited presence of B-doped G domains and C-doped h-BN and BNC boundaries by dehydrogenation and pyrolitic decomposition of DMAB on Pt(111). This method can be potentially used for band gap engineering and applications in devices. The temperature is the principal parameter to selectively grow the *h*-BNG layer in competition with hybridized B-C-N layers on the clean crystal surface (S. Nappini et al. paper in preparation).

In this paper we investigate the nearly freestanding *h*-BNG layer on Pt(111) by core level x-ray photoemission (XPS), near-edge absorption spectroscopy (NEXAFS), temperature programmed desorption (TPD), low energy electron microscopy (LEEM) combined to X-ray photoemission electron microscopy (XPEEM). The spatially resolved measurements are complemented with micro-spot electron energy loss spectroscopy (μ-EELS) and low energy electron diffraction (μ-LEED) data.

We have grown the in-plane *h*-BNG layer in UHV dosing 150 L of commercial dimethylamine borane (Sigma Aldrich, 97%) molecules on a (111)-terminated platinum single crystal held at different temperatures. 1000 K was found to be the optimal substrate temperature to get the most ordered and flat surface.

2. Results and Discussion

The LEED pattern (**Figure 1**) is characterized by the principal hexagonal Pt(111)-(1×1) diffraction spots surrounded by sharp non-integer moiré satellites and an arc-shaped

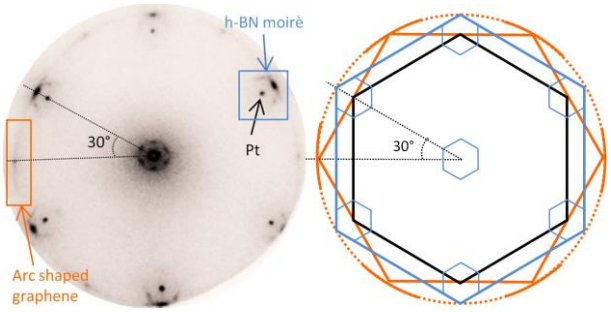

Figure 1. Left panel: LEED pattern of *h*-BNG layer on Pt(111) at 1000 K recorded with electron energy E_0 = 60 eV. h-BN moiré, graphene and Pt spots are identified by the corresponding labels. The distortion is due to imperfect diffraction imaging conditions in our instrument. Right panel: scheme of the LEED pattern; black hexagon represents the first-order diffraction of Pt(111) substrate, the yellow circle is due to the first-order diffraction of graphene domains, with a preferential distribution (solid orange curves) around the 30° rotated domains (orange hexagon), the light blue hexagons represent the h-BN first-order diffraction and h-BN moiré.

diffraction pattern rotated by 30° from the (1×1) Pt diffraction spots. The moiré satellites appear as a hexagonal network of diffraction spots external to the substrate pattern and with identical orientation. The distance ratio between first order substrate reflections and external hexagonal-network spots is approximately 9:10. An analogous superstructure was also reported for h-BN/Pt(111) layer obtained by borazine precursor at the same temperature of the substrate[13,14]. This similarity suggests that the moiré satellites can be ascribed to the presence of long-range-ordered domains of h-BN aligned parallel to the substrate lattice. The arc-shaped diffraction pattern centered at 30° from the Pt(1×1) spots points towards the formation of G domains with different azimuthal orientations in agreement with other works reporting G growth on Pt(111) at the same temperature[15,16].

The local order of the in-plane *h*-BNG layer grown on Pt(111) was investigated by LEEM and μ-LEED. The presence of a heterostructure is revealed by LEEM micrographs in bright field (BF) (see **Figure 2a** and **a'**), where a clear image contrast between darker and brighter complementary areas is ascribable to the presence of two phases on the sample. The two

regions display different electron reflectivity curves at low electron energy pointing to distinct

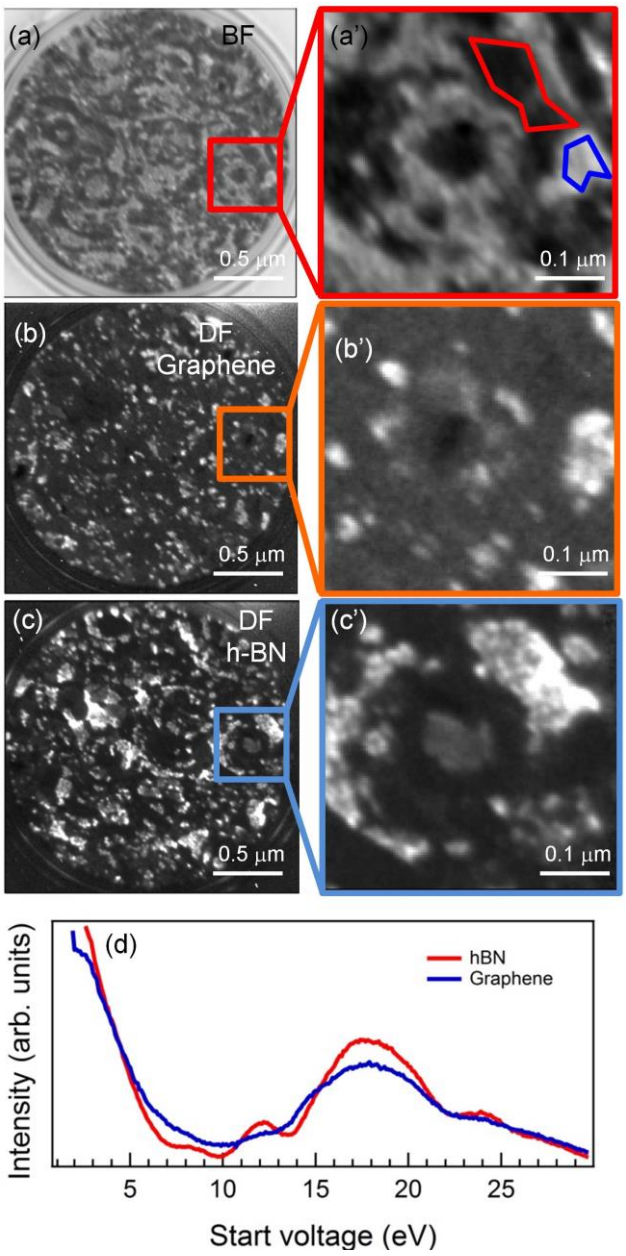

Figure 2. Left LEEM images of *h*-BNG layer on Pt(111) at 1000 K. (a) Bright Field LEEM at V_{start} = 6 eV. The red square indicates the zoomed area (a'). (b) Dark Field LEEM image using the graphene first-order diffraction spot of 30° rotated domains (V_{start} =35 eV). The orange square indicates the zoomed area (b'). (c) Dark Field LEEM image using the *h*-BN first-order diffraction (V_{start} =35 eV). The light blue square indicates the zoomed area (c'). (d) LEEM (IV) characteristics obtained from a stack of LEEM images with electron energy from 2 to 30 eV at the locations marked in (a').

structures. As we will show further below using spectromicroscopy measurements, one area

corresponds to G, whereas the other to *h*-BN.

Dark field (DF) LEEM was used to correlate the LEED pattern to real space surface structure. Representative DF images obtained using the first order of diffraction of *h*-BN and G spots are reported in **Figure 2** (**b, c, b', c'**). In contrast to BF, DF LEEM is sensitive to the rotational alignment. DF image measured selecting the *h*-BN first-diffraction order spot show many bright irregularly shaped areas of a few hundred nm size. In the DF image taken on the center of the G ring-like spot (at 30° from the first-order Pt diffraction spots) smaller bright regions are observed. The two DF images are only partially complementary; this is more evident by the comparison of the zoomed images **Figure 2b'** and **2c'** where the inversion of contrast is not total. This is not surprising considering that G domains have different azimuthal orientations, as it is evident from the ring-like LEED pattern. On the contrary, the BF (**Figure 2a** and **2a'**) and DF images on *h*-BN (**Figure 2c** and **2c'**) display a contrast inversion. This is a confirmation of almost identical azimuthal orientation of all the *h*-BN domains with respect to the substrate lattice as derived from the moiré satellites spots observed in the LEED pattern.

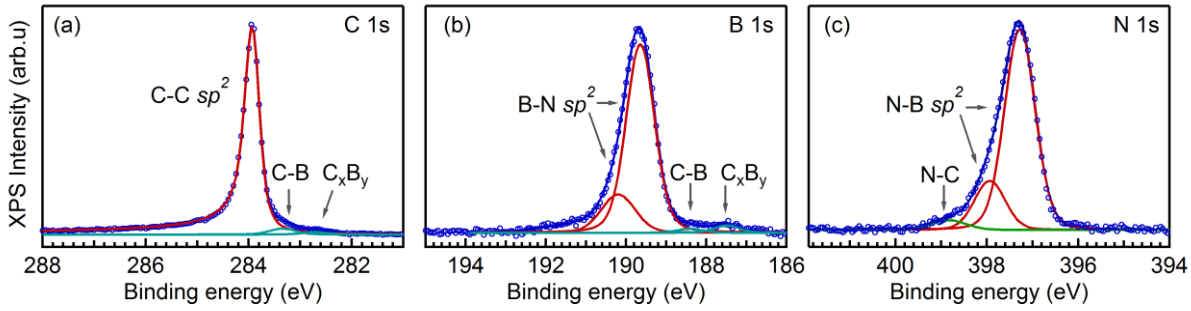

Figure 3. C 1s (a), B 1s (b), and N 1s (c) high-resolution x-ray photoemission spectra of the *h*-BNG layer prepared on the Pt(111) substrate at a temperature of 1000 K. The x-ray excitation energy was set to 520 eV.

High-resolution core-level x-ray photoelectron spectroscopy provides an indication on the *h*-BNG heterostructure formation, its structure on Pt(111), the strength of the interaction of this layer with the substrate and between *h*-BN and G domains. Both N 1s and B 1s spectra display slightly asymmetric peak shapes (**Figure 3**). This asymmetric peak shape has been simulated by two components, a main peak at 189.7 eV and 397.3 eV for N 1s and B 1s,

respectively, and a second weaker component at binding energies of 190.1 eV and 397.9 eV, respectively. The presence of very similar photoemission features in B 1s and N 1s core levels was also observed in *h*-BN/Pt(111) layers and, in this case, the weak components at higher binding energy (BE) were assigned to a small geometrical corrugation of the *h*-BN domains produced by different interaction of the N and B atoms with the Pt(111) substrate when they are placed on different atomic sites[17].

The N 1s spectrum exhibits also a third weak component at a BE of 398.9 eV (**Figure 3c**). An increase of this component was observed after dosing DMAB at temperatures below 1000 K (not shown) and it can be assigned to pyridine-like nitrogen impurities in the G domains[18,19] or to N atoms at the boundaries between *h*-BN and G domains[3,6]. In the B 1s spectrum (**Figure 3b**), traces of B–C bonds can be found at lower binding energies. Two weak components at 188.4 eV and 187.5 eV can be attributed to B-doping in carbon nanoparticles or G[20,21] or B–C bonds at the *h*–BN/G boundaries[3] and to nonstoichiometric B_xC_y boron carbide[20]. Corresponding B–C components in C 1s spectrum are present at 283.4 and 282.6 eV, respectively (**Figure 3a**). Their contribution to the whole C 1s peak is 3%. The C 1s spectrum is dominated by a sharp peak at 283.9 eV assigned to sp^2 hybridized C atoms in G[22]. From our investigation of the layers prepared at lower temperatures (not shown) a component around 286.1 eV, related to the N–C bonds is also likely present, but it is obscured by the tail of the asymmetric Doniach–Šunjić line shape of the main peak.

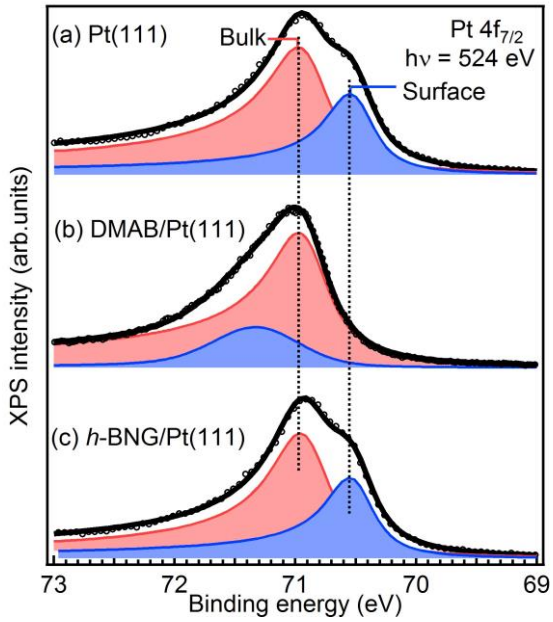

Figure 4. Pt $4f_{7/2}$ photoemission spectra of (a) the clean Pt(111) surface, (b) Pt surface exposed to dimethylamine borane at room temperature, and (c) surface covered by the *h*-BNG layer. The spectra were decomposed into components corresponding to photoemission from bulk and surface top-most platinum atoms.

By measuring the Pt 4f emission at high-energy resolution, information about the strength of the chemical interaction at the Pt interface with the *h*-BNG layer can be accessed. For clean metals, the lower coordination of the atoms at the surface leads to a different core-level binding energy components compared to the bulk. This can be observed in **Figure 4a** where the Pt $4f_{7/2}$ spectrum measured on clean Pt(111) can be decomposed in two components, one centered at 70.90 eV (Pt bulk atoms), a second shifted by 0.40 eV towards lower BE (Pt surface atoms), in good agreement with the literature[23–25].

Upon exposure to DMAB molecules keeping the substrate at room temperature, the surface component is completely reduced, whereas a new peak at 71.30 eV appears (**Figure 4b**). The large shift of the surface component to higher BE value implies a chemical interaction of Pt with the DMAB adsorbate. The appearance of a new component located at higher binding energy have been observed for other organic molecules, e.g. Zn-Pc [26], propene, ethylidine, 2-butenal, CCH_3 [27,28], with an adsorbate-induced surface core level shift up to 0.36 eV."

On the contrary, after the formation of the *h*-BNG layer at 1000 K, the Pt $4f_{7/2}$ spectrum can be well fitted with the same peak components as in the case of clean Pt(111) surface (**Figure 4c**). This is indicative of a very weak interaction and suggests that the *h*-BNG layer is almost free standing on the Pt(111) surface.

X-PEEM measurements of the Pt 4f, C 1s, B 1s and N 1s core level emission (**Figure 5 a, b, c, d**) confirm the presence of laterally separate *h*-BN and G regions, which cover the substrate in a continuous manner. In fact, a total inverted contrast in the XPEEM images of B 1s and N 1s images with respect to C 1s ones can be observed, while the image obtained with Pt $4f_{7/2}$ shows uniform intensity over the entire area.

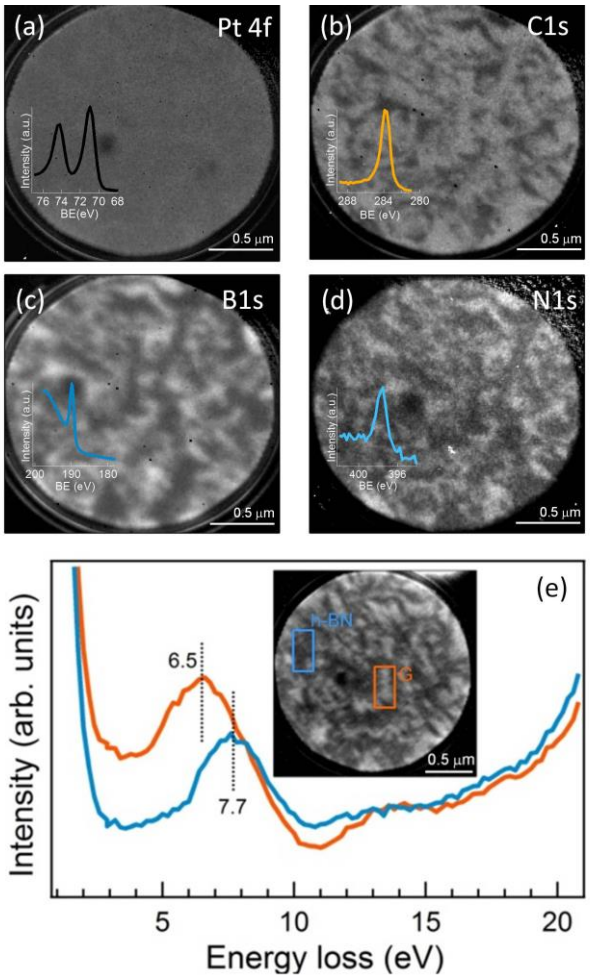

Figure 5. XPEEM images at the (a) Pt $4f_{7/2}$, (b) C1s, (c) B 1s and (d) N1s core levels. Pt 4f and B 1s were recorded using a photon energy of 260 eV, N 1s and C 1s using a photon energy of 520 eV. The inset on bottom left of each image is the core level spectrum obtained by integrating the signal on the whole field of view through a stack of XPEEM images measured at different kinetic energy of the photoemitted electrons. (e) Electron energy loss

spectra recorded from the areas labeled A (orange circle) and B (light blue circle) in the Energy-filtered BF LEEM image reported in the inset. The image was collected with electron energy E_0 = 32 eV; the graphene patches appear bright, the *h*-BN dark. The spectrum measured in region A shows a π- plasmon loss at 6.5 eV; the spectrum measured in region B shows the π- plasmon loss around 7.7 eV.

X-PEEM measurements of the Pt $4f_{7/2}$ core level (**Figure 5 a**) indicate that, within the lateral resolution of the instrument, all the Pt surface is covered by single layer *h*-BNG, without any bi- or multi-layer domains. This conclusion is further supported by the energy-dependent low energy electron reflectivity measurements in the real space (LEEM I(V) data shown in **Figure 2d**) measured on G and *h*-BN domains separately.

LEEM I(V) gives a clear fingerprint of the number of layers in G since mono-, bi- and multi-layers display very different I(V) characteristics[15]. The strong similarity of the present μ-LEEM-I(V) measurements on individual G domains with the published LEEM I(V) measurements from a nearly free standing monolayer G on Pt(111) and Ir(111)[29,30] clearly excludes the presence of bi- and multi-layers.

The LEEM instrument used for this experiment is equipped with an energy filter, enabling to obtain spatially resolved electron energy loss spectroscopy (μ-EELS) measurements. A good way to probe the electronic structure of the *h*-BNG layer is the measurement of the excitation of surface plasmons[31]. The π plasmon is a sensitive probe of G band structure near the Fermi level as observed e.g. in the work by Shin and coworkers[32] who followed in single layer G the modifications induced on π-plasmon by charge doping and layer thickness. The plasmon loss is also very sensitive to the interaction of the G layer with the substrate, as observed by Oida et al.[33] in G grown on SiC(0001). In the latter case, when G layer is covalently bonded to the substrate no plasmon loss is observed. **Figure 5e** reports the EELS spectra obtained integrating the signal on a bright region (orange curve) and on a dark region (light blue curve) of the BF LEEM image shown in the inset of **Figure 5**. The BF LEEM image is measured with incident electron energy of 32 eV and scattering geometry with both the incident and scattered beams normal to the surface (q||=0). The analysis reveals that on the bright area,

assigned to G, the collective excitation of the electrons is found at 6.5 eV , whereas on the dark area, assigned to *h*-BN, a peak centered at 7.7 eV is found. The π-plasmon energy loss measured for G in the present work is slightly larger than the values reported in literature for pure single-layer non-interacting G layer, measured in similar geometrical conditions. For pure G/Pt(111)[34] and for G/SiC (0001) after decoupling of the G layer from the covalently bonded substrate by oxidation[33] a value of 6.2 eV is reported. This discrepancy supports the fact that in our case the electronic properties of G are modified by the presence of atomic doping. In particular, according to Shin et al.[32], a shift of about 0.3 eV toward higher energy corresponds to a n-doping of about 5×10^{13} electrons/cm^2, which could be attributed to the presence in G of an excess amount of nitrogen donors of about 1%.

The plasmon energy loss measured on the dark regions at 7.7 eV is different from the value calculated (6 eV) for single layer *h*-BN[35,36], but the observed energy position is in good agreement with the 7.5 eV peak experimentally observed in *h*-BN exfoliated flakes[36]. Following the calculation of Pan et al.[36], the observed energy position can be explained considering the presence of impurities in the *h*-BN layer. In our case, as already observed in the photoemission data, the *h*-BN electronic properties are partly modified by the orbital mixing inside or at the boundaries between *h*-BN with G domains.

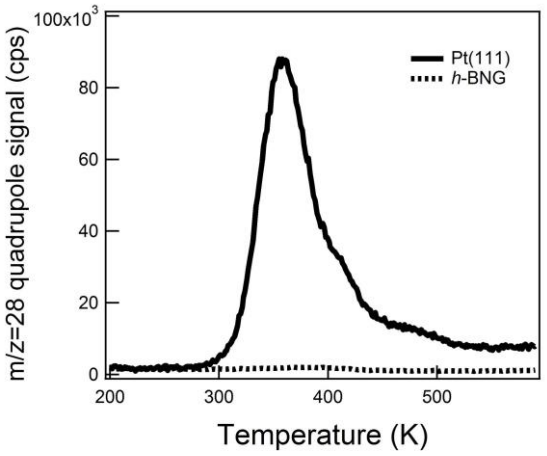

Figure 6. TPD desorption spectra of 12 L CO (1.3×10^{-7} mbar 2 min) dosed at 150 K on clean Pt(111) (solid curve) and on *h*-BNG (dotted curve).

As we have reported above, all the spectromicroscopy data point to the existence of a continuous coverage of laterally distinct G and *h*-BN domains. In order to confirm that there are no uncovered Pt atoms below the lateral resolution limit (about 30 nm) of our microscopy setup, we have performed thermal programmed desorption (TPD) measurements. CO desorption spectra recorded after 12 Langmuir CO exposure at 150 K, show no CO desorption peak for *h*-BNG up to 600 K, whereas for Pt(111) there is a clear desorption peak centered at 360 K (see **Figure 6**). This indicates that the Pt(111) substrate is perfectly covered by the composite layer[37] and possible phase boundaries must be continuous at atomic level and do not present significant voids exposing Pt sites.

The layer continuity readily translates into a lowered reactivity against adsorbates, and in particular to oxygen. To demonstrate the oxidation resistance of *h*-BNG, C 1s, N 1s and B 1s core levels were acquired after exposing the layer to a partial pressure of O_2 (up to 5×10^{-6} mbar for 200 s) at different temperatures of the substrate (300 K, 500 K, 600 K) and no changes have been observed (not shown). This indicates that the *h*-BNG layer is chemically inert as G and *h*-BN.

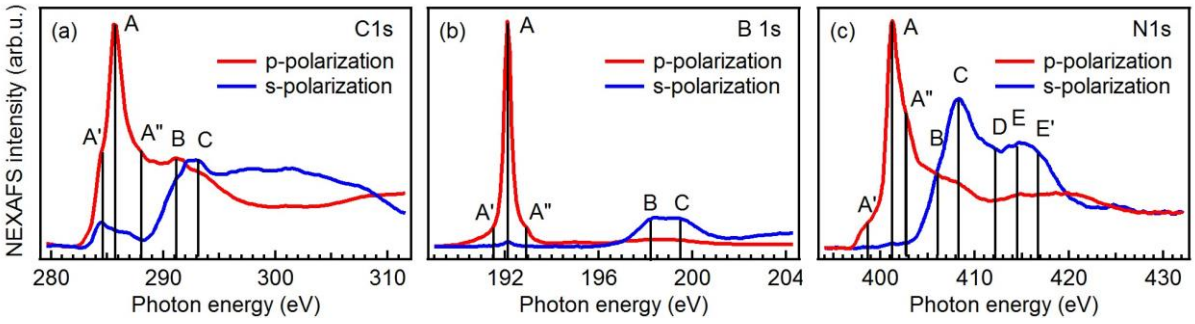

Figure 7. Polarization dependent NEXAFS spectra at (a) C K, (b) B K, and (c) N K edge from the *h*-BNG layer. Red curves correspond to p-polarization and blue curves to s-like polarization geometry

Polarization-dependent NEXAFS is used to get information on the structure and orbital hybridization of the layer. **Figure 7** shows the spectra from the *h*-BNG layer at C, B and N K-edges measured using linearly polarized radiation incident with two different angles between

polarization vector and surface plane: normal incidence geometry (Θ = 0°, s-polarization) and near grazing incidence geometry (Θ = 60°, p-like polarization). As expected for layered systems, the polarization dependence is very pronounced, thus allowing us to easily distinguish between π* states (features labeled as A', A, A'') and σ* states (B, C, D, E, E') of the hybrid *h*-BNG layer. For C K-edge NEXAFS spectra the overall spectrum profiles are very similar to the ones measured for pure G/Pt(111)[25,38]. The main absorption peak selected with p-polarization corresponds to π* states, while the continuous absorption at higher photon energies is assigned to σ* states. The polarization dependence shows that the π* states are suppressed using s-polarized light, as expected for flat and ordered G domains on Pt(111)[25]. Also B and N K-edge NEXAFS spectra are very similar to those measured for pure *h*-BN on Pt(111)[14]. The disappearance of the π*-related structures going from p- to s-polarization both in B K- and N K-edge NEXAFS spectra indicates that also *h*-BN domains are nearly flat. However, *h*-BNG show small but significant differences in NEXAFS spectra with respect to those from pure G[25,38] and *h*-BN[14] on Pt(111), indicating a different chemical state.

In the present *h*-BNG system C, B and N K-edge NEXAFS spectra show an increased intensity of the features A' and A" in the π* state and a partial broadening of the σ* structures (B, C, D, E, E') with respect to the single pure systems G/Pt(111) and *h*-BN/Pt(111)[14,38]. Generally, the A' and A" shoulders at the π* states appear when G and *h*-BN[14,38] have a stronger interaction with the substrate, and it is often accompanied by a strong broadening of the σ* states.

However, this hypothesis is not applicable to our case, considering the evidence of a very weak interaction between Pt and *h*-BNG layer indicated by Pt 4f core levels. The presence or increased intensity of the A' and A" features and the weak broadening of σ* states in C K-edge and in B and N-K edges can be originated by orbital mixing inside or at the boundaries between *h*-BN with G domains[39], consistent with what found in μ-EELS and core level photoemission.

3. Conclusion

A novel growth procedure is reported to obtain an almost free standing in-plane layer mostly composed by G and *h*-BN domains on Pt(111) using a single molecular precursor. LEEM measurements indicate that both G and *h*-BN domains can be as large as a few hundred nm. LEEM, in agreement with TPD, XPS and XPEEM, show that the layer fully covers the Pt substrate and there are no voids exposing Pt sites. High-resolution photoemission core levels prove that the layer has a very weak interaction with the substrate and is inert to oxidation, and highlight the presence, although limited to small areas, of BNC hybrid domains. Angle-dependent NEXAFS spectra show that both G and *h*-BN domains are flat, but display slight differences with respect to G and *h*-BN layers on Pt(111) that can be associated to orbital mixing inside or at the boundaries between domains.

4. Experimental Section

Sample preparation: The sample was prepared at the BACH beamline in an ultra-high vacuum (UHV) chamber with a base pressure of 3×10^{-10} mbar connected to the spectroscopy chamber. The Pt(111) single crystal (MaTecK, GmbH, 99.999% purity) was prepared with cycles of sputtering at 1.5 kV at 300 K, annealing at 925 K in the 2×10^{-7} mbar O_2 partial pressure and flash annealing to 1025 K in UHV. All temperatures were measured by a thermocouple in direct contact with the sample. The sample cleanliness was checked using photoemission spectroscopy, monitoring the absence of any contaminant, in particular C 1s and O 1s core level peaks, in surface sensitive conditions (kinetic energy around 230 eV and 105 eV for C 1s and O 1s respectively and 60° grazing emission). The degree of the long-range order on the surface was monitored by low-energy electron diffraction (LEED). The Pt $4f_{7/2}$ and graphene (G) C 1s photoemission spectra were fitted with Doniach–Šunjić (DS) line

shapes convoluted with Gaussian function. N 1s and B 1s photoemission spectra were decomposed into the spectral components using Voigt function line shapes. A Shirley type background was subtracted from Pt $4f_{7/2}$, C 1s and N 1s spectra and a linear background from the B 1s spectrum.

Dimethylamine borane (DMAB) (Sigma Aldrich, 97.0%), purified by several cool-pump-heat cycles, was dosed (6.65×10^{-7} mbar for 300 s) via a leak valve from a glass tube kept at 41°C on the Pt substrate held at 1000 K .

XPS and NEXAFS measurements: X-ray photoelectron spectroscopy (XPS) and near-edge x-ray absorption spectroscopy (NEXAFS) measurements were carried out in an UHV multi-spectroscopy endstation of the CNR beamline BACH at the synchrotron facility Elettra (Trieste, Italy) on the same sample prepared in-situ. The data were acquired using a VG-Scienta R3000 hemispherical analyzer. The overall energy resolution for core levels was set to 0.2 eV for XPS and 0.1 eV for NEXAFS spectra. The NEXAFS spectra were measured in Auger electron yield mode (AEY) collecting the KVV Auger-electrons with the electron energy analyzer and the intensities were normalized to the photon beam flux, measured by the drain current on a reference golden grid. Polarization-dependent measurements were performed by rotating the sample between normal incidence geometry (angle between the sample surface plane and x-ray polarization vector $\theta = 0°$, s-polarization) and grazing incidence geometry ($\theta = 60°$, p-like polarization).

LEEM, X-PEEM measurements: Low-energy electron microscopy (LEEM), including intensity-voltage I(V) LEEM measurements using the specular beam (0 0), x-ray photoemission electron microscopy (X-PEEM) and micro-electron energy loss spectroscopy (μ-EELS) measurements were performed at the Nanospectroscopy beamline (Elettra - Sincrotrone Trieste). For the microscopy measurements the same sample was prepared ex-situ after an annealing at 350 °C in UHV. Nanospectroscopy beamline operates a state-of-the-art spectroscopic photoemission and low-energy electron microscope (SPELEEM) equipped with

an energy-filter. The instrument combines LEEM and X-PEEM techniques, which provide structural and chemical sensitivity, respectively.

In the SPELEEM, the electron kinetic energy is controlled by biasing the sample with a negative potential referred to a start voltage, V_{start}. In our measurements, LEEM was used in both bright and dark-field (BF and DF) modes, respectively, utilizing the first or secondary order diffraction beams for imaging. The microscope lateral resolution approaches 10 nm in LEEM mode and 30 nm in XPEEM; energy resolution is better than 0.3 eV in imaging spectroscopy. Along with imaging, the SPELEEM allows diffraction operation mode. In this mode, the probed area is restricted to a micron-sized region by inserting a field-limiting aperture in the image plane.

TPD measurements: TPD experiments were carried out in a custom made UHV system operating at a base pressure of 10^{-10} mbar equipped with a Hiden quadrupole mass spectrometer, and facilities for LEED, photoemission spectroscopy and sample preparation. In order to analyze the desorption species coming only from the sample surface, the quadrupole spectrometer, covered by a quartz shield holding bearing a 6 mm wide sampling aperture, was placed at 5 mm from the Pt(111) single crystal, which was suspended by two (2 mm diameter) tantalum wires. Sample temperature was determined by a type K thermocouple spot welded on the back of the sample. For all experiments we used a heating rate of 2 K/sec.

Acknowledgements
This work was supported by CNR and the Italian MIUR through the national grant Futuro in Ricerca 2012 RBFR128BEC “Beyond graphene: tailored C-layers for novel catalytic materials and green chemistry”, by MIUR through the program `Progetto Premiale 2012' - Project ABNANOTECH, and by the University of Padova funded project: CPDA128318/12 “Study of the catalytic activity of complex graphene nanoarchitectures from ideal to real conditions”. Federico Salvador and Paolo Bertoch are acknowledged for technical support. We gratefully thank A. Locatelli for his valuable input during the laterally-resolved measurements and data analysis.

Received: ((will be filled in by the editorial staff))
Revised: ((will be filled in by the editorial staff))
Published online: ((will be filled in by the editorial staff))

[1] M. P. Levendorf, C.-J. Kim, L. Brown, P. Y. Huang, R. W. Havener, D. A. Muller, J. Park, *Nature* **2012**, *488*, 627.

[2] S. Haldar, P. Srivastava, O. Eriksson, P. Sen, B. Sanyal, *J. Phys. Chem. C* **2013**, *117*, 21763.

[3] L. Ci, L. Song, C. Jin, D. Jariwala, D. Wu, Y. Li, A. Srivastava, Z. F. Wang, K. Storr, L. Balicas, F. Liu, P. M. Ajayan, *Nat. Mater.* **2010**, *9*, 430.

[4] B. Muchharla, A. Pathak, Z. Liu, L. Song, T. Jayasekera, S. Kar, R. Vajtai, L. Balicas, P. M. Ajayan, S. Talapatra, N. Ali, *Nano Lett.* **2013**, *13*, 3476.

[5] Y. Gong, G. Shi, Z. Zhang, W. Zhou, J. Jung, W. Gao, L. Ma, Y. Yang, S. Yang, G. You, R. Vajtai, Q. Xu, A. H. MacDonald, B. I. Yakobson, J. Lou, Z. Liu, P. M. Ajayan, *Nat. Commun.* **2014**, *5*.

[6] C.-K. Chang, S. Kataria, C.-C. Kuo, A. Ganguly, B.-Y. Wang, J.-Y. Hwang, K.-J. Huang, W.-H. Yang, S.-B. Wang, C.-H. Chuang, M. Chen, C.-I. Huang, W.-F. Pong, K.-J. Song, S.-J. Chang, J.-H. Guo, Y. Tai, M. Tsujimoto, S. Isoda, C.-W. Chen, L.-C. Chen, K.-H. Chen, *ACS Nano* **2013**, *7*, 1333.

[7] M. Liu, Y. Li, P. Chen, J. Sun, D. Ma, Q. Li, T. Gao, Y. Gao, Z. Cheng, X. Qiu, Y. Fang, Y. Zhang, Z. Liu, *Nano Lett.* **2014**, *14*, 6342.

[8] P. Sutter, R. Cortes, J. Lahiri, E. Sutter, *Nano Lett.* **2012**, *12*, 4869.

[9] J. Lu, L. C. Gomes, R. W. Nunes, A. H. Castro Neto, K. P. Loh, *Nano Lett.* **2014**, *14*, 5133.

[10] L. Liu, J. Park, D. A. Siegel, K. F. McCarty, K. W. Clark, W. Deng, L. Basile, J. C. Idrobo, A.-P. Li, G. Gu, *Science* **2014**, *343*, 163.

[11] T. Gao, X. Song, H. Du, Y. Nie, Y. Chen, Q. Ji, J. Sun, Y. Yang, Y. Zhang, Z. Liu, *Nat. Commun.* **2015**, *6*.

[12] Y. Gao, Y. Zhang, P. Chen, Y. Li, M. Liu, T. Gao, D. Ma, Y. Chen, Z. Cheng, X. Qiu, W. Duan, Z. Liu, *Nano Lett.* **2013**, *13*, 3439.

[13] M. T. Paffett, R. J. Simonson, P. Papin, R. T. Paine, *Surf. Sci.* **1990**, *232*, 286.

[14] A. B. Preobrajenski, A. S. Vinogradov, M. L. Ng, E. Ćavar, R. Westerström, A. Mikkelsen, E. Lundgren, N. Mårtensson, *Phys. Rev. B* **2007**, *75*, 245412.

[15] P. Sutter, J. T. Sadowski, E. Sutter, *Phys. Rev. B* **2009**, *80*, 245411.

[16] M. Gao, Y. Pan, L. Huang, H. Hu, L. Z. Zhang, H. M. Guo, S. X. Du, H.-J. Gao, *Appl. Phys. Lett.* **2011**, *98*, 033101.

[17] E. Ćavar, R. Westerström, A. Mikkelsen, E. Lundgren, A. S. Vinogradov, M. L. Ng, A. B. Preobrajenski, A. A. Zakharov, N. Mårtensson, *Surf. Sci.* **2008**, *602*, 1722.

[18] D. Usachov, O. Vilkov, A. Grüneis, D. Haberer, A. Fedorov, V. K. Adamchuk, A. B. Preobrajenski, P. Dudin, A. Barinov, M. Oehzelt, C. Laubschat, D. V. Vyalikh, *Nano Lett.* **2011**, *11*, 5401.

[19] J. Jin, F. Pan, L. Jiang, X. Fu, A. Liang, Z. Wei, J. Zhang, G. Sun, *ACS Nano* **2014**, *8*, 3313.

[20] M. Cattelan, S. Agnoli, M. Favaro, D. Garoli, F. Romanato, M. Meneghetti, A. Barinov, P. Dudin, G. Granozzi, *Chem. Mater.* **2013**, *25*, 1490.

[21] J. Gebhardt, R. J. Koch, W. Zhao, O. Höfert, K. Gotterbarm, S. Mammadov, C. Papp, A. Görling, H.-P. Steinrück, T. Seyller, *Phys. Rev. B* **2013**, *87*, 155437.

[22] M. Cattelan, G. W. Peng, E. Cavaliere, L. Artiglia, A. Barinov, L. T. Roling, M. Favaro, I. Píš, S. Nappini, E. Magnano, F. Bondino, L. Gavioli, S. Agnoli, M. Mavrikakis, G. Granozzi, *Nanoscale* **2015**, *7*, 2450.

[23] L. Bianchettin, A. Baraldi, S. de Gironcoli, E. Vesselli, S. Lizzit, L. Petaccia, G. Comelli, R. Rosei, *J. Chem. Phys.* **2008**, *128*, 114706.

[24] M. L. Ng, R. Balog, L. Hornekær, A. B. Preobrajenski, N. A. Vinogradov, N. Mårtensson, K. Schulte, *J. Phys. Chem. C* **2010**, *114*, 18559.

[25] S. Rajasekaran, S. Kaya, T. Anniyev, H. Ogasawara, A. Nilsson, *Phys. Rev. B* **2012**, *85*, 045419.

[26] S. Ahmadi,_ B. Agnarsson, I. Bidermane, B. M. Wojek, Q. Noël, C. H. Sun, and M. Göthelid, *J. Chem. Phys.* **2014**, *140*, 174702

[27] E. Janin, S. Ringler, J. Weissenrieder, T. _Akermark, U. O. Karlsson, M. Göthelid, D. Nordlund, and H. Ogasawara, *Surf. Sci.* **2001** 482-485, 83

[28] O. Björneholm, A. Nilsson, H. Tillborg, P. Bennich, A. Sandell, B. Hernn • as, C. Puglia, and N. Mårtensson, Surf. Sci. **1994** 315, L983

[29] P. Sutter, J. T. Sadowski, E. Sutter, *Phys. Rev. B* **2009**, *80*, 245411.

[30] A. T. N'Diaye, R. van Gastel, A. J. Martínez-Galera, J. Coraux, H. Hattab, D. Wall, F.-J. M. zu Heringdorf, M. H. Hoegen, J. M. Gómez-Rodríguez, B. Poelsema, C. Busse, T. Michely, *New J. Phys.* **2009**, *11*, 113056.

[31] R. M. Tromp, Y. Fujikawa, J. B. Hannon, A. W. Ellis, A. Berghaus, O. Schaff, *J. Phys. Condens. Matter* **2009**, *21*, 314007.

[32] S. Y. Shin, N. D. Kim, J. G. Kim, K. S. Kim, D. Y. Noh, K. S. Kim, J. W. Chung, *Appl. Phys. Lett.* **2011**, *99*, 082110.

[33] S. Oida, F. R. McFeely, J. B. Hannon, R. M. Tromp, M. Copel, Z. Chen, Y. Sun, D. B. Farmer, J. Yurkas, *Phys. Rev. B* **2010**, *82*, 041411.

[34] A. Politano, A. R. Marino, V. Formoso, D. Farías, R. Miranda, G. Chiarello, *Plasmonics* **2011**, *7*, 369.

[35] A. G. Marinopoulos, L. Wirtz, A. Marini, V. Olevano, A. Rubio, L. Reining, *Appl. Phys. A* **2004**, *78*, 1157.

[36] C. T. Pan, R. R. Nair, U. Bangert, Q. Ramasse, R. Jalil, R. Zan, C. R. Seabourne, A. J. Scott, *Phys. Rev. B* **2012**, *85*, 045440.

[37] M. Cattelan, E. Cavaliere, L. Artiglia, L. Gavioli, S. Agnoli, G. Granozzi, *Surf. Sci.* **2015**, *634*, 49.

[38] A. B. Preobrajenski, M. L. Ng, A. S. Vinogradov, N. Mårtensson, *Phys. Rev. B* **2008**, *78*, 073401.

[39] T. Schiros, D. Nordlund, L. Pálová, D. Prezzi, L. Zhao, K. S. Kim, U. Wurstbauer, C. Gutiérrez, D. Delongchamp, C. Jaye, D. Fischer, H. Ogasawara, L. G. M. Pettersson, D. R. Reichman, P. Kim, M. S. Hybertsen, A. N. Pasupathy, *Nano Lett.* **2012**, *12*, 4025.